A verified solution of friction factor in compression test based on its sample's shape changes

Khoddam, S.; Fardi, M.; Solhjoo, S.

Published in:
International Journal of Mechanical Sciences

DOI:
10.1016/j.ijmecsci.2020.106175

Publication date:
2021

International Journal of Mechanical Sciences 193 (2021) 106175

Contents lists available at ScienceDirect

International Journal of Mechanical Sciences

journal homepage: www.elsevier.com/locate/ijmecsci

A verified solution of friction factor in compression test based on its sample's shape changes

S. Khoddam [a,*], M. Fardi [b], S. Solhjoo [c]

[a] Institute for Frontier Materials, Deakin University, Geelong, Victoria, Australia, 3216
[b] Department of Mechanical & Aerospace Engineering, Monash University, Clayton, VIC 3800, Australia
[c] Computational Mechanical and Materials Engineering, Engineering and Technology Institute Groningen, Faculty of Science and Engineering, University of Groningen, Nijenborg 4, 9747 AG Groningen, the Netherlands

ARTICLE INFO

Keywords:
Friction factor
contact
kinematic solution
foldover
compression test

ABSTRACT

The friction factor is a key input for "barrel compression test" and for a meaningful interpretation of the test data. Despite its widespread use, due to the complexity of the problem, there are very few solutions available for the test, let alone for the friction factor. Extended-Avitzur (EA) model has serious known limitations to calculate the friction factor. To estimate the friction factor more reliably, a closed-form solution of the friction factor has been proposed here. The solution is based on the "Exponential Profile Model" (EPM) and provides an instantaneous value for the friction factor. It simply relies on the sample's initial and deformed dimensions. Unlike existing experimental procedures, the proposed solution integrates the test results and friction factor identification based on a single set of experimental load-displacement-barreling data. Merits of the model and its solution were highlighted and compared to those of the conventional Cylindrical Profile Models (CPMs). A finite element model was developed as the reference to produce pseudo-experimental test data and to verify the presented solution. The deformation data were used in the EPM and the EA model to calculate the friction factors by each model and to compare them with the reference data as the benchmark. Contrary to EA's estimated friction factors, those identified by the EPM were in good agreement with the reference values. Recommendations were provided to identify a deformation zone at which the EPM's friction factor can be estimated meaningfully.

Introduction

Friction is a complex phenomenon with numerous key roles and applications in science and engineering. Prior knowledge of *friction factor* is also essential for several experimental-numerical studies [1–7], industrial forming processes [8–12] and characterization material properties [12–16]. Solving friction's exact governing equations for a real transient process or its physical simulation is extremely complex.

"Barrel Compression Test" (BCT), also known as Axisymmetric Compression Test, is extensively used by researchers to physically simulate friction and deformation to understand their associated phenomena, particularly to characterize the flow behaviour of materials in hot and cold forming conditions and to design and optimize industrial forming processes.

As far as the BCT applications are concerned, there are two essential initiatives to estimate friction factor more accurately:

1 As a material property characterization tool, BCT heavily relies on the accuracy of its post-processing techniques to convert the raw data into the flow curves. The flow curves are then studied and analysed to understand other related phenomena (e.g. recovery, static/dynamic/meta-dynamic recrystallization).
2 The test is an important avenue to understand friction behaviour and its development during industrial processes that are physically simulated by BCT.

The test provides two avenues to study friction; no barreling, and with barreling. The latter can be classified in three groups; analytical geometry-based, experimental geometry-based and numerical. A timeline of the selected analytical works on BCT's no barreling and with barreling and their developments are shown in Fig. 1 and discussed next.

No barreling (Cylindrical) 1950-1967: Nadai [28] presented one of the earliest solutions of the test which ignores the effects of barreling in the deforming sample. A no barreling solution, also known as a Cylindrical Profile Model (CPM), ignores the shear deformation in the sample and replaces the barrelled profile by an equivalent cylindrical one. The solution is incapable of estimating the friction and employs a constant friction factor as a pre-known value.

Conventional CPM solutions employ a bi-linear velocity field with several oversimplifications most notably on the exclusion of shear de-

* Corresponding author.
E-mail address: shahin@deakin.edu.au (S. Khoddam).

https://doi.org/10.1016/j.ijmecsci.2020.106175
Received 1 September 2020; Received in revised form 12 October 2020; Accepted 25 October 2020
Available online 28 October 2020
0020-7403/

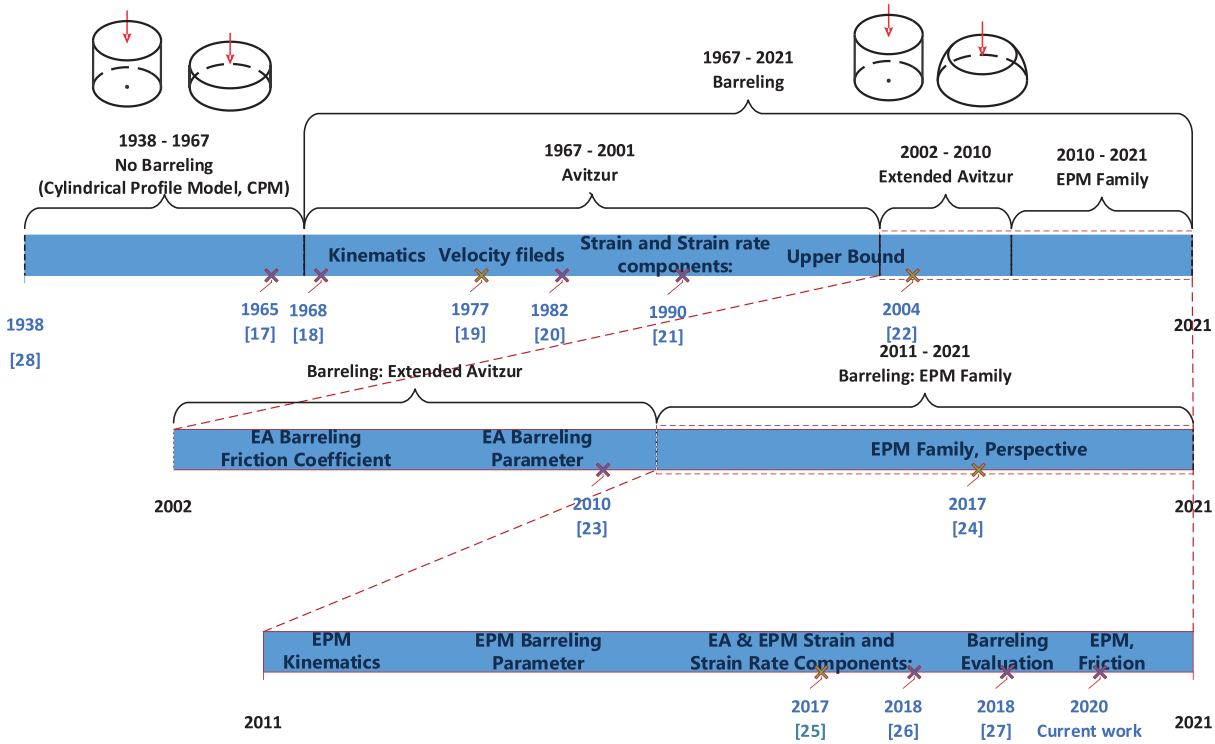

Fig. 1. A time-line of BCT's selected analytical milestones from no-barreling to barreling era; [17–28] and the current work.

formation in the sample and assumptions on friction; they require friction factor as a pre-requisite to convert the measured load-displacement data to the material flow data. Another limitation is that an average friction factor has to be identified separately through another experiment before being used to interpret the compression test measurements (see for example [29,30] and [14]). This uncoupled procedure significantly increases the labour and uncertainties in the obtained flow data.

Due to the simplicity of the CPM solutions, they are still being widely used beyond their scope e.g. for thermo-mechanical processing and studies. The validity of these works can be disputed elsewhere. In more than five decades, several researchers have attempted to establish a reliable theoretical and experimental technique to estimate friction. Key examples of these techniques include the works done by Kobayashi and Thomsen [17] and Avitzur [21] who are among the pioneers of such endeavours.

Avitzur Family, 1967-2001 (with Barreling): This era has two stages: *Avitzur, 1967-2*001 and *Extended Avitzur, 2002-1010* which are discussed next.

Avitzur, 1967-2001: Avitzur's limit analysis (Avitzur [19]) and its associated upper bound solution of BCT, provided key pioneering developments for barreling studies. The work entailed a dedicated kinetically admissible velocity field incorporating a barreling parameter which was used to define shearing deformation in the sample through a barreling parameter. The resulted strain rate components were employed in an upper bound solution of the problem. These attempts almost coincided with the advent of numerical methods such as finite element analysis [31] and their applications to solve complex boundary value problems. The promises of finite element are at least partially responsible to postpone closed-form solutions of the test for a while; the numerical methods appeared shortly as attractive and powerful alternatives to closed-form solutions of the problems, see for example [32–34]. However, due to the numerical solutions' need to the material properties and friction factor as inputs, the solutions were deemed unqualified as viable "direct techniques" to characterize the most important process parameters. Nevertheless, numerical solutions are considered the best available methods to simulate such complex problems and to benchmark their solutions.

Extended Avitzur (EA), 2002-2010: Ebrahimi and Najafizadeh [22] extended Avitzur's upper bound solution to a new level. They utilized a solution for Avitzur's barreling parameter to indirectly measure the test's friction factor based on the initial and deformed dimensions of BCT sample. We refer to this model as Extended-Avitzur (EA) model. Khoddam and Hodgson [25] found that EA formulation provides a reasonably good estimation of effective strain and strain rate in the sample when compared to those based on CPM solutions. Due to EA's convenience, its friction factor has been extensively used by researchers to identify materials flow behaviours based on CPM solutions. However, as shown by Solhjoo [23] in a comparative study, the EA's predicted friction factor deviates significantly with those simulated by finite element. In an attempt to rectify this, Solhjoo developed some alternative solutions ([23] and [35]) to identify the parameter more accurately and eventually its associated friction factor. Unfortunately, neither of the proposed alternatives provided a reliable estimate of the friction factor. These led the authors to a conclusion that Avitur's kinematically admissible velocity field is not representative enough for the barreling test and therefore the family of Avitzur-based solutions, including EA, are unqualified for friction factor identification. One notes the challenging and iterative nature of an upper bound based friction solution which can only be verified after completion of all previous theoretical layers including velocity filed, kinematic solution and upper bound solutions. This is a result of the non-uniqueness of the admissible velocity field for a boundary value problem; a kinematically admissible velocity field does not guarantee a reliable friction solution. A remedy for the non-uniqueness issue is to iterate alternative kinematically admissible velocity fields; an optimum velocity field can be found by verification. Such an iteration will eventually provide a reliable *new family* of upper bound solution for friction factor. This explains why the authors proposed a new family of formulation (see EPM family in Fig. 1) which is explained next.

Exponential Profile Model (EPM) Family (with Barreling), 2011-now: The end of the EA solution era meant a need to propose new alternatives. To accomplish this, a new model: Exponential Profile Model (EPM) was proposed by Khoddam; EPM's family of formulations was

briefly outlined in [24]. EPM's associated sets of theoretical layers (EPM's family) included its alternative barreling parameter [27], kinematic solution, strain rate components [26] and deformation energy [27]. The theories were developed in preparation for an upper bound-based solution for the test's friction factor. The latter is EPM's inner-most theoretical layer and will be dealt with in the current work and verified against a reference numerical solution.

Experimental geometry-based solution of BCT's friction: Sofuoglu and Gedikli [30] proposed an experimental procedure for the measurement for friction compensation, ring compression test and the open-die backward extrusion test technique. Also, Jung, Lee, Kim, Kang and Im [36] used the tip test to measure the friction during cold forging. However, these procedures are often difficult to perform and they don't directly nor adequately represent the friction in a real forming process. It is not practical to run a separate measurement for each BCT.

Numerical friction studies on BCT: Inverse (indirect) approaches have been used to identify deformation related parameters and friction. Examples of these are parameter identification for plain strain processes [37], an indirect measurement of static recrystallization [38] and constitutive parameters by Zhao, Wang, Chang and Yan [39]. More recent examples can be found in [40–42]. However, these procedures are quite pruned to entrapment into a local minimum during their optimization steps [43–45].

A combination of FEA and an analytical solution has been extensively used in the literature to explain microstructural evolution during physical testings. An example of this is the study of flow and microstructure [46]. The results obtained by an ill-defined mixed approach should be used with care as they may not be transferable to the industrial processes. Li, Onodera and Chiba [47] developed an alternative method to evaluate the friction factor by curve fitting the FE simulated test results. However, the derivations have limited usage and are mostly applicable to the simulated cases.

This work fills the gap for a verified analytical solution of BCT's friction factor. This geometry-based solution, which relies on the EPM velocity field, provides an alternative BCT solution for indirect measurement of the friction factor based on the sample geometry changes. The solution involves the derivation of the deformation power and frictional power loss in the sample in an upper bound framework using the EPM's kinematic solution. Next, a closed-form solution for BCT's friction factor is derived by minimization of a "minimum potential energy functional" for EPM's barreling parameter. This will be followed by validation of the proposed solution using an FE model as the reference. Also, EA solutions for the same scenarios will be presented to allow a comparison between the merits of each model and their solutions.

Theoretical derivations for BCT's friction factor

A concise summary of BCT's terms and definitions

A unified set of symbols are used for the geometry of the barrelled sample, its velocity field and strain rate components are presented first to allow an easier cross-referencing between the current work and the previous literature. The terminologies and symbols are used next to derive a closed-form solution of friction factor based on EPM's kinematic solution.

The barreled geometry

The conventional no-barreled model of BCT, "Cylindrical Profile Model" (CPM) is shown in Fig. 2 and compared with the barreled model. A CPM model ignores "*barreling induced deformation*" of its free surface assuming that its profile remains cylindrical during the test. Due to its simplicity, it has been frequently used in the literature (e.g. [48–50]).

Undeformed geometry of BCT sample and its coordinate system, (r, z) are shown in Fig. 2a. This is a classical disc compression problem with a solid sample being compressed between two parallel rigid platens. The no-barreled sample's profile at an arbitrary time step, $t_n \neq 0$, is shown in Fig. 2b in which shearing deformation is ignored. The same deformation step, $t_n \neq 0$, is shown in Fig. 2c with a barrelled profile taking into account the shearing deformation. Key geometrical parameters for both models and their coordinate systems are also shown in the same figures. For both models, the radial and tangential axes of the cylindrical coordinate system are located in the samples mid-plane. In practice, the upper platen moves towards the lower one with a downward velocity $\dot{H}$, which is held fixed. For ease of formulation, we fix the coordinate system's r axis to the mid-plane with centre, O, located at the sample's centre. This, however, doesn't change the problem and based on this representation, sample's top and bottom surface velocities are now $-0.5\dot{H}$ and $0.5\dot{H}$, toward the mid-plane, respectively. Consequently, the problem becomes symmetric in both geometry and loading and therefore, only the upper half of the sample needs to be solved. Also, it is assumed that the sample does not rotate; the tangential coordinate, θ, is excluded in Fig. 2 for simplicity. However, we note that a nonzero shearing strain develops in the planes containing the third axis.

The radial, axial and tangential scalar components of displacement for a material point in the barreled sample are denoted by u, v and w, respectively, and the same symbols with a "dot superscript" represent their corresponding velocity components. The tangential components w and $\dot{w}$ are not shown in Fig. 2 for the sake of simplicity.

For the case of CPM (Fig. 2b), sample's profile radius, $\bar{R}_n = 0.5D_0\sqrt{\frac{H_0}{H_n}}$, is assumed constant across z direction for the given deformation step n.

The incremental and generic time steps

Due to the plastic nature of deformation and the presence of friction, deformation energy transfer during BCT is *non-conservative*. As a result, the process becomes *path dependant*. For an easier presentation of the transient deformation and friction during BCT, two time-step conventions are adopted throughout this article: *incremental* and *generic* notations. Presenting different expressions in this article, a deformation or friction parameter is frequently referred to with emphasize on its time-step, n when it is evaluated or measured. Such cases are presented in this article using an "*incremental notation*".

Different solutions of the barreled sample including geometrical, velocity field, strain and strain rate components and upper bound energy terms can be performed incrementally or generically. Solutions for both small and large deformation increments in EPM were presented in [26] and [27], respectively. The latter is suitable to identify the EMP's instantaneous barreling parameter and its profile, $R_n(z)$. Fig. 2c illustrates the barrelled radius, $R_n(z)$ at the sample's free surface at a time step of n in a given $r-\theta$ plane parallel to the mid-plane as a function of z. The radius has an arbitrary axial distance of z from the mid-plane.

Example parameters of BCT, to be represented either as incremental or generic, are $R_n(z)$, D_n and H_n (see Fig. 2) which denote instantaneous profile radius, mid-plane diameter and height corresponding to a time step n, respectively. An incremental expression typically correlates the parameters between two quasi-static sequential time steps namely n and $n-1$. Otherwise, the same parameter may be referred to using a *generic notation* when the incremental nature of the process is less emphasized. An example is when the deformation step is near the undeformed configuration ($n=0$). When using the generic notation, the current time step subscript (n) is dropped for the sake of brevity. This simplifies the upcoming formulations. When an expression is represented by generic notations, the body's configuration is compared to the initial configurations denoted by subscripts 0 (e.g. D_0 and H_0).

Friction factor identification; energy conservation

This section provides an interpretation of the well-known "conservation of energy" principle applied to "compression of a solid disk" as a "non-conservative (non-ideal)" process. It also allows to use a consistent

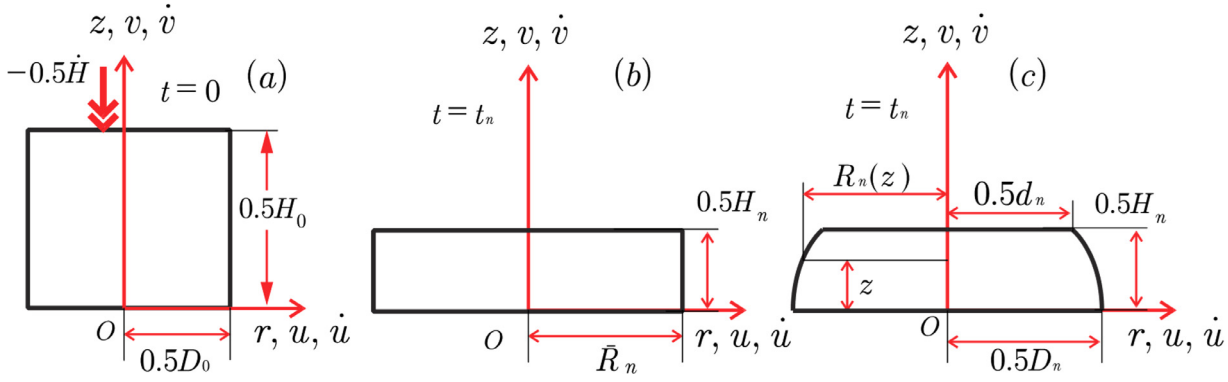

Fig. 2. Illustration of a compression increment; (a) undeformed-initial sample, (b) ignoring barreling (CPM) an arbitrary deformed-cylindrical ($t=t_n$)- showing an arbitrary cylindrical profile radius $\bar{R}_n$ (profile's effective radius) and (c) barrelled profile ($t=t_n$)- showing an arbitrary $R_n(z)$ (barrelled profile's radius).

nomenclature for parameters used in these well-known principles, those used in metal forming and those already used in EPM formulation.

A deforming BCT sample may be considered as a non-isolated system separated from its environment at its two boundaries namely sample tool's interface and sample's free surface. The conservation of energy can be stated mathematically for the BCT system: a change in the system's total energy ΔE_{sys}, is equal to the total sum of energy transferred across the system boundary ΣT by some mechanism (e.g. work or heat) during the change (see for example [51]:

$$\Delta E_{\text{sys}} = \Delta U_{int} + \Delta E_{tr} = \sum T \tag{1}$$

where ΔU_{int} and ΔE_{tr} are the internal energy change due to plastic strain and traction induced energy change at the tool-sample interface due to friction, respectively. We note that both $\Delta U_{int}$and ΔE_{tr} are irreversible. Assuming an isothermal system, the only mechanism of energy transfer in this system is the work across the tool-sample interface ΣT. For a small quasi-static height change of ΔH, the work is $\Sigma T = L\Delta H$ where L is the contact force between the tool and sample. Dividing both sides of Eq. 1 by an infinitesimal time increment of $\Delta t = t_n - t_{n\text{-}1}$, an expression for *conservation of power* can be written as the following well-known form (see for example [18] or [52]):

$$\dot{E}_{\text{sys}} = \dot{U}_{int} + \dot{U}_{tr} = \int_V \bar{\sigma}\sqrt{\frac{2}{3}\dot{\epsilon}_{ij}\dot{\epsilon}_{ij}}dV + \int_S T_i.\phi_i dS = L\dot{H} \tag{2}$$

where $\dot{U}_{int} = \Delta U_{int}/\Delta t$ and $\dot{U}_{tr} = \Delta E_{tr}/\Delta t$ are internal deformation power and traction power, respectively and $\sum T/\Delta t = L\dot{H}$. In Eq. 2, $\dot{U}_{int}$ represents the power consumed (changed) in the system due to the plastic deformation and $\dot{U}_{tr}$ stands for the power associated with the frictional tractions. Also, volume V denotes the deforming barrelled domain, S is the area of that boundary where the tractions (friction-induced shearing stresses) develop and $\bar{\sigma}$ is the material's effective stress (von-Mises' yields strength). Under an ideal deformation, without friction, it is typically assumed that the effective strain, strain rate and stress are homogeneous and internal deformation energy changes only due to plastic deformation. To account for the irreversibility of the process due to friction and plastic deformation, described by Eq. 2, we impose some more realistic assumptions: effective strain and strain rate changes heterogeneously in V, effective stress is homogeneous, and both internal deformation energy changes due to plastic deformation and traction power and deformation energy changes due to elastic deformation are ignored. In Eq. 2, the integrals have to be taken over the actual strain-path due to the presence of friction forces and plastic deformation in the system. The integrand $T_i.\Phi_i$ is the scalar product of the external traction T_i and the material velocity Φ_i over the traction boundary S. The right-hand side of Eq. 2 is the total sum of power transferred across the boundaries by the mechanism of work rate by the contact force L.

EPM's total potential energy

The term $\int_V \bar{\sigma}\sqrt{2/3\dot{\epsilon}_{ij}\dot{\epsilon}_{ij}}dV$ in Eq. 2 can be found by a change of variables as $dV = 2\pi r dr dz$.

Substituting EPM's expression for effective strain rate $\dot{\epsilon}$ (see [26] for the derivations) and rearranging the terms:

$$\dot{U}_{int} = \frac{4\pi\bar{\sigma}\dot{H}}{\sqrt{3}H^2}\int_{z=0}^{0.5H}\int_{r=0}^{\bar{R}} 2r\sqrt{(1-2BH)^2r^2 + 3(BH(H-4z)+2z)^2}dr dz \tag{3}$$

where B is EPM's barreling parameter [26].

Eq. 3 is expressed using the generic notation. Its upper limit of integral, $\bar{R}$, is an imaginary *effective radius*, $\bar{R} = 0.5D_0\sqrt{\frac{H_0}{H}}$ which is defined based on a volume constancy assumption. Integrating and simplifying, $\dot{U}_{int}$ in Eq. 3 can be found as:

$$\dot{U}_{int} = \pi\bar{\sigma}\dot{H}\beta \tag{4}$$

$$\beta = \frac{1}{6\sqrt{3}H^2\gamma_1^3}\left(H\left(6\Gamma_1 - \Gamma_2 + \Gamma_3\right) + \Gamma_4\right) \tag{5}$$

In which:

$$\gamma_1 = 1 - 2BH \tag{6}$$

$$\Gamma_1 = \sqrt{3}BH\left(B^2H^4\right)^{3/2} - \sqrt{3}\gamma_2\left(H^2\gamma_2^2\right)^{3/2} \tag{7}$$

$$\gamma_2 = 1 - BH \tag{8}$$

$$\Gamma_2 = BH\ \gamma_3\left(6B^2H^4 + 5\bar{R}^2\gamma_1^2\right) \tag{9}$$

$$\gamma_3 = \sqrt{3B^2H^4 + \gamma_1^2\bar{R}^2} \tag{10}$$

$$\Gamma_3 = \gamma_2\ \gamma_4\left(6H^2\gamma_2^2 + 5\bar{R}^2\gamma_1^2\right) \tag{11}$$

$$\gamma_4 = \sqrt{3H^2\gamma_2^2 + \gamma_1^2\bar{R}^2} \tag{12}$$

$$\Gamma_4 = \sqrt{3}\bar{R}^4\left(\ln\left(\sqrt{3}\ \gamma_3 - 3BH^2\right) - \ln\left(\sqrt{3}\ \gamma_4 - 3H\gamma_2\right)\right)\gamma_1^4 \tag{13}$$

The eight new terms defined in Eqs. 6 to 13 are introduced to avoid a lengthy-expression for β in Eq. 4 and to allow its calculation in a multi-step fashion. The term β is an instantaneous geometrical parameter whose dimension is $[L^2]$ and can be physically interpreted as an imaginary deforming area in the sample.

The friction shear stress at the sample-die interface is most commonly expressed as μP_{ave} or as mk where μ and m $(0 \le m \le 1)$ are

called "Coulomb's coefficient of friction" and "friction factor", respectively. P_{ave} is compressive normal stress to the interface and k is the shear strength of the deforming material. An approximate correlation between μ and m can be made based on a CPM based analysis.

In this work, we calculate the traction power loss, $\dot{U}_{tr}$, in terms of *friction factor* which represents friction during metal forming studies better than *Coulomb's coefficient*.

Assuming the von-Mises yield criterion for the sample, the traction power loss, $\dot{U}_{tr}$, is usually calculated in metal forming (see for example [53]) using the following expression for the friction traction (shearing stress) between a platen and the sample:

$$T_i = mk = \frac{m\bar{\sigma}}{\sqrt{3}} \tag{14}$$

where m is the friction factor and k is material's shear yield strength. The material velocity, φ_i, at the traction boundary S, is:

$$\phi_i = \dot{u}|_{z=0.5H} = \dot{u}|_{z=-0.5H} = \left(B + \frac{1-2BH}{H}\right)r\dot{H} \tag{15}$$

Changing the variable, $dS_3 = 2\pi r dr$, and replacing the values, one can find $\dot{U}_{tr}$ as:

$$\dot{U}_{tr} = \int_S T_i.\phi_i dS_3 = 2\int_0^{\bar{R}} \frac{m\bar{\sigma}}{\sqrt{3}}\left(B + \frac{1-2BH}{H}\right)r\dot{H}2\pi r dr = \frac{4\pi m\bar{R}^3(1-BH)\bar{\sigma}\dot{H}}{3\sqrt{3}} \tag{16}$$

The velocity difference between the platens and the sample in the direction of shear and parallel to the platen surface in Eq. 16 was accounted twice as S comprises the upper and lower interfaces. The power transferred across the tool-sample interface to the system is $L_{EPM}\dot{H}$. Equations 4 and 16 are substituted in Eq. 2 which results in:

$$L_{EPM}\dot{H} = \pi\bar{\sigma}\dot{H}\beta + \frac{4\pi m R^3(1-BH)\bar{\sigma}\dot{H}}{3\sqrt{3}} \tag{17}$$

or:

$$L_{EPM} = \pi\bar{\sigma}\left(\beta + \frac{4mR^3(1-BH)}{3\sqrt{3}}\right) \tag{18}$$

where L_{EPM} is the contact force between the tool and sample according to EPM theory. Friction factor, m, is a key pre-requisite in Eq. 18 to convert BCT's test results in flow stress based on EPM. In what follows, Eq. 18 is used in an optimization framework to identify the friction factor.

A solution for ***m*** *using the minimum total potential energy*

The *minimum total potential energy principle* states that the actual velocity solution is a kinematically admissible velocity field that satisfies the following conditions:

- fulfils the governing equations
- renders a stationary total potential energy, when only the primary variable changes; the velocity field brings the system's total energy at a stationary state when *an infinitesimal variation* δ from such a state along with the primary variable results no change in the energy.

A careful examination of Eq. 18 shows that the right-hand side is proportional to the consumed power in the sample, $\dot{E}_{sys}$, and has the barreling parameter B as the only variable for a given deformed configuration. In other words, B is the primary variable in Eq. 18 and therefore the equation can be considered as the following functional Π -see for example Kupradze and Aleksidze [54] - which represents the total power consumed in the system:

$$\Pi = \beta + \frac{4mR^3(1-BH)}{3\sqrt{3}} \propto \dot{E}_{sys} \tag{19}$$

Dividing the left-hand side terms in Eq. 1 by Δt changes its nature from total energy change into total power. Likewise, the total potential energy principle can be restated as the variation of total power, $\delta\dot{E}_{sys}$ or $\delta\Pi$, and expressed mathematically as:

$$\delta\Pi = \delta\dot{U}_{int} + \delta\dot{U}_{tr} = 0 \tag{20}$$

when only the primary variable B changes.

In a numerical solution of BCT, the first condition is fulfilled when the velocity boundary conditions are applied and the second condition is fulfilled in an iterative form. For EPM's velocity field presented in this work [26], we note that the first and second conditions have already been satisfied. To fulfil the third condition, we treat barreling parameter, B, as the primary variable. Minimizing the functional Π with respect to B satisfies the third condition by calibrating the velocity field for the deformed configuration under consideration. This can be physically interpreted as follows, during an ideal deformation process the minimum energy corresponds to the minimum barreling. To find the instantaneous value of m for the current deformed configuration, Eq. 20 can be restated by eliminating the functional's first derivative with respect to B:

$$\frac{\partial\Pi}{\partial B} = \frac{\partial\dot{U}_{int}}{\partial B} + \frac{\partial\dot{U}_{tr}}{\partial B} = 0 \tag{21}$$

The symbolic solution for friction factor, m, in the generic notation can be presented as follows (see Appendix A for details):

$$m = \frac{H\left(\Omega_1 - \Omega_2 + \Omega_3 + \Omega_4\right) - \Omega_5}{4H\gamma_1^4\bar{R}^3} \tag{22}$$

where the following five new terms are also defined to abbreviate Eq. 22 further:

$$\Omega_1 = -6H^2\left(\sqrt{3}\sqrt{H^2\gamma_2^2} - \gamma_4\right) - \bar{R}^2\left(4\,\gamma_3 + \gamma_4\right) \tag{23}$$

$$\Omega_2 = 2B^3H^3 \left(3H^2\left(\sqrt{3}\sqrt{B^2H^4} + \sqrt{3}\sqrt{H^2\gamma_2^2} - \gamma_3 - \gamma_4\right) - 10\bar{R}^2\left(\gamma_3 + \gamma_4\right)\right) \tag{24}$$

$$\Omega_3 = 6B^2H^2 \left(H^2\left(2\sqrt{3}\sqrt{B^2H^4} + \sqrt{3}\sqrt{H^2\gamma_2^2} - 2\,\gamma_3 - \gamma_4\right) - 2\bar{R}^2\left(3\,\gamma_3 + 2\gamma_4\right)\right) \tag{25}$$

$$\Omega_4 = 3BH\left(2H^2\left(\sqrt{3}\sqrt{H^2\gamma_2^2} - \gamma_4\right) + \bar{R}^2\left(7\,\gamma_3 + 3\gamma_4\right)\right) \tag{26}$$

$$\Omega_5 = \sqrt{3}\gamma_1^4\bar{R}^4\left(\ln\left(\sqrt{3}\,\gamma_3 - 3BH^2\right) - \ln\left(\sqrt{3}\gamma_4 - 3H\gamma_2\right)\right) \tag{27}$$

where γ_1, γ_2, γ_3 and γ_4 were defined in Eqs. 6 to 12.

A careful examination of Eq. 22 shows that it correlates the friction factor m with the instantaneous geometrical measures namely B, H and $\bar{R}$, which are specific to the deformed configuration of the test sample. Thus, the calculated m based on Eq. 22 varies with deformation. This is in agreement with the experimental findings by Wang and Ramaekers [55] for the plane strain compression test and by Han [56] for BCT on the instantaneous nature of m. In fact, Rastegaev test specimen for BCT [57] was proposed by a few researchers (e.g. [58]) to avoid the increase in m during the test but its laborious procedure proved to be unpractical.

The solution described by Eq. 22 provides an instantaneous value of m provided that the barrelling data (instantaneous d, D and H) are available since the start of deformation. This is due to the irreversible nature of friction and plastic deformation which makes the process path dependant.

Based on Eq. 22, to monitor the changes in m when deformation is progressing, the test rig has to record the mid-plane diameter D simultaneously with other test data (e.g. H and L). Concurrent measurement of D requires to add a diameter transducer [59] to the test rig. Equation 22 indicates that the conventional practices of BCT which are based on an assumed and fixed value of m to interpret the test results (e.g. CPM) are not justified.

Table 1
Summary of sample's barreling data obtained by FEA simulation [23]; D, d, $\bar{R} = R$ and H are given in *mm*.

		FEM's friction factor; m_{FEA}									
		0.1	**0.2**	**0.3**	**0.4**	**0.5**	**0.6**	**0.7**	**0.8**	**0.9**	**1.0**
H = 15, $\bar{R}$ = 5.164	0.5D	5.174	5.186	5.196	5.201	5.204	5.207	5.209	5.211	5.213	5.214
	0.5d	5.122	5.095	5.076	5.063	5.054	5.0460	5.040	5.034	5.028	5.023
H = 13, $\bar{R}$ = 5.547	0.5D	5.549	5.577	5.600	5.619	5.634	5.6480	5.656	5.663	5.668	5.668
	0.5d	5.438	5.373	5.318	5.271	5.230	5.1930	5.160	5.123	5.107	5.090
H = 11, $\bar{R}$ = 6.030	0.5D	6.037	6.093	5.960	6.162	6.184	6.2020	6.213	6.221	6.226	6.229
	0.5d	5.832	5.714	5.515	5.554	5.504	5.4720	5.475	5.404	5.395	5.369
H = 9, $\bar{R}$ = 6.667	0.5D	6.674	6.757	6.811	6.847	6.875	6.8960	6.909	6.920	6.924	6.927
	0.5d	6.365	6.223	6.126	6.067	5.994	5.9180	5.932	5.930	5.925	5.910
H = 8, $\bar{R}$ = 7.0711	0.5D	7.0750	7.1690	7.2270	7.2660	7.2950	7.3160	7.3310	7.3420	7.3480	7.3510
	0.5d	6.7140	6.5860	6.4550	6.3980	6.3680	6.2950	6.2510	6.2490	6.2230	6.1910

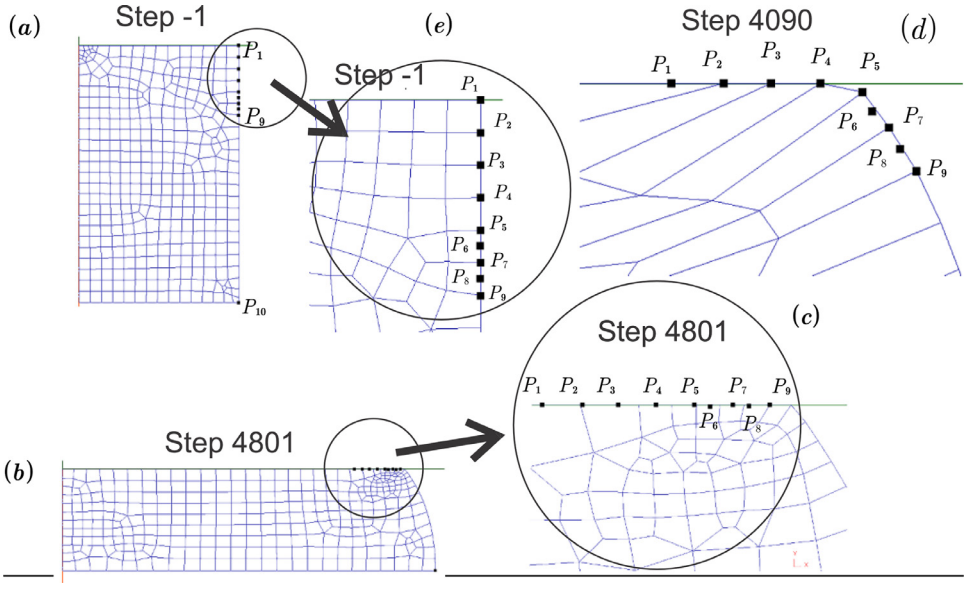

Fig. 3. Use of tracking nodes to extract $d-H$ data from the FEA solutions; the position of (a) the chosen 10 tracking nodes on the initial mesh, (b) the 9 tracking points on the fully deformed mesh, (c) the tracking points on an intermediate mesh. (e) and (c) are the insets of (a) and (b), respectively. (d) shows the tracking point at the end of deformation.

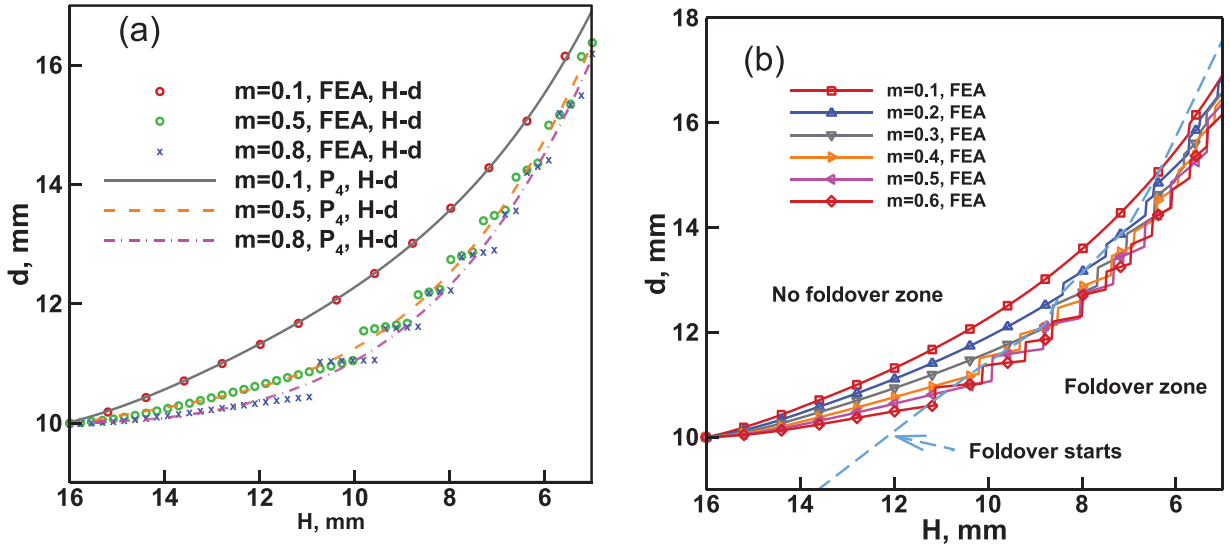

Fig. 4. (a) Smoothening of the numerical $H-d$ data using the 4th order polynomials and (b) Onset of foldover and its development with friction factor m.

On numerical verification of EPM's friction solution

The key input into Eq. 22 is the barreling parameter B which can be indirectly measured [27] based on the concurrently measured $H-D-d$ data. For various reasons, obtaining this data during the test is challenging. Further, such an experiment doesn't allow verification of the identified friction factor. To avoid these, we adopt a virtual experiment to generate the required pseudo data and to check the accuracy of the identified friction factor using Eq. 22. An FE model is constructed to generate the set of pseudo-experimental $H-D-d$ for the test scenarios. The FE model and data generation will be discussed in the next section.

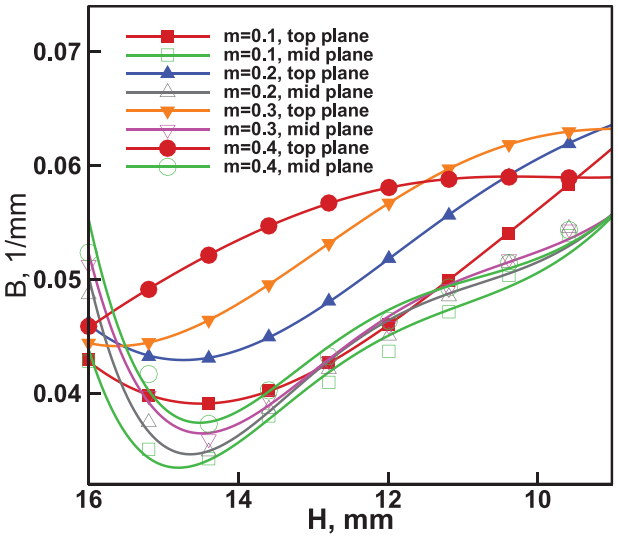

Fig. 5. Barreling parameter B estimated based on the FE results at the top and mid-planes of the sample and their variations with H and m.

Incompressibility is a key concern when enforcing the minimum total potential energy principle and solving the friction factor. Numerical solution of Eq. 2 enforces the incompressibility by adding a penalty term using a penalty constant or a Lagrange multiplier. A method used here is to include the incompressibility in EPM indirectly by estimating the instantaneous value of B based on a method presented in [27] which relies on the top-plane diameter d. This results in indirect incorporation of the measured d and therefore indirect enforcement of the incompressibility in the solution. Hence, the pseudo $H-d$ data become critical to estimate m by EPM.

BCT's finite element model

A finite element model is developed using SFTC-DEFORM Premier ™ software to generate the pseudo-experimental data. The deformation data will be used as input data to compute friction factors by EA and EPM solution expressed by Eq. 22. Finally, the friction factors are compared with those of the experimental data.

The constructed Finite Element model of BCT was solved for a series of BCT case studies. This allowed a correlation of friction and geometrical parameters of the deformed sample. To make the results comparable with those published by Solhjoo [23], in the first set of simulations we adopted a similar test scenario with: $D_0 = 10mm$, $H_0 = 16mm$, $H = 15$ to 8 mm with 1 mm steps and $m_{FEA} =$ 0.1 to 1 with 0.1 steps.

For all cases solutions presented here, the coordinates shown in Fig. 2 was chosen. Due to the axisymmetric nature of the problem, only a quarter of each test sample and a rigid upper die was modelled using 460 quadrilateral bi-linear elements and 517 nodes. During the simulations, the upper die was moved with a given speed along the negative z-axis to deform the sample positioned between the moving upper die and the r-axis as the symmetry axis.

A previous study by Fardi et al [24] using two FEM programs DEFORM 2D and ABAQUS showed that "the geometry-based" calculation of friction factor is not highly sensitive to the material property nor the test temperature. As such, the choice of material behaviour should have minimum impact on the calculated values of m. The two materials used in our simulations merely represent two case studies and based on the conclusions of the above study, we expect that the findings based on other material types will be the same.

In the first set of finite element simulations by Solhjoo [23], Al-6063 samples with a composition of Si=0.44, Cu=0.05, Mn=0.05, Mg=0.47, Cr=0.03, Zn=0.1, Ti=0.01, Fe=0.20 and Al=balance at an isothermal temperature of 200°C were simulated based on the material properties provided in the program's library [36]. The material exhibits a strong work hardening behaviour in contrast with Al-1100 which behaves almost in a rigid perfectly plastic fashion with a low work hardening rate.

In the second set of finite element simulations, Al-1100 samples with a composition of Si=0.19, Cu=0.10, Mn= 0.01, Mg=0.01, Fe=0.50, Al=balance at the same isothermal condition were used based on the material properties provided in the program's library [37] to ensure that the calculated m according to Eq. 22 applies to both types of materials.

For each simulation, a constant friction factor (m_{FEA}), was chosen and the resulting D and d were recorded. The values of D, d, and m for the first set of finite element simulations are listed in Table 1 for comparison.

A note on the pseudo-experimental $H-D-d$ data

During the sample deformation, due to the friction-induced consequent barreling, the upper part of the specimen profile may form a new contact surface with the die. This phenomenon is known as foldover which complicates the generation of the pseudo data. Exclusion of the

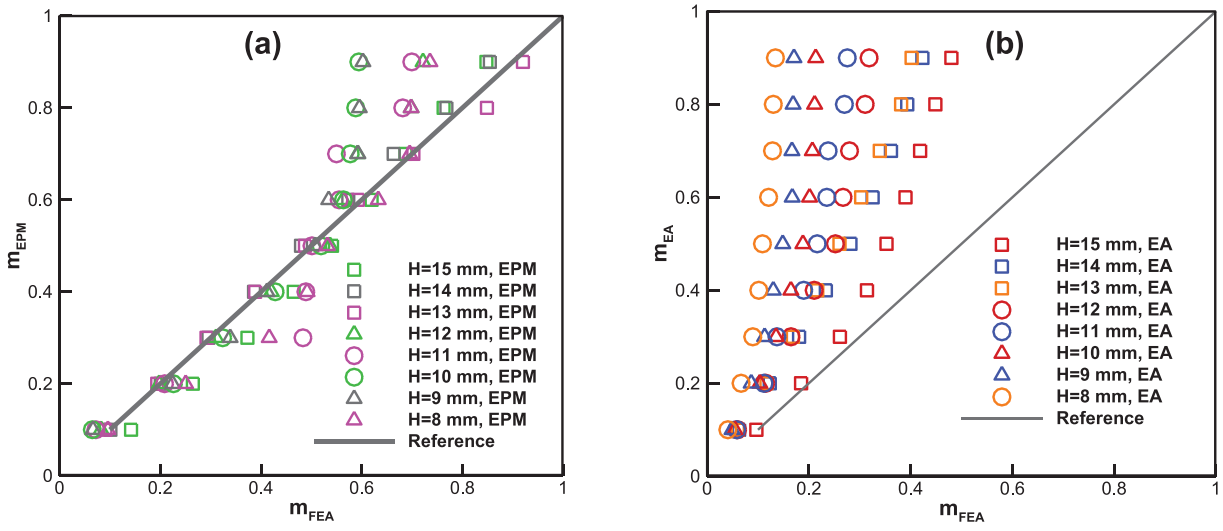

Fig. 6. Comparing friction factor m_{EPM} and m_{EA} calculate by EPM and EA methods, respectively with their counterparts in FEA simulation, m_{FEA}; (a) EPM and (b) EA's method [23]. A generic approach has been adopted in these calculations.

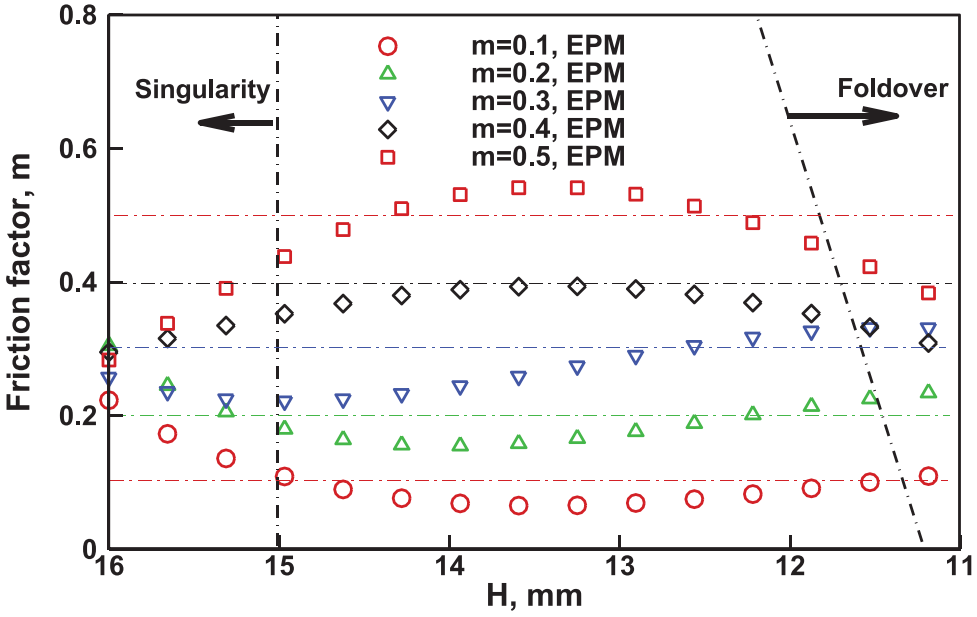

Fig. 7. Comparison of m values based on EPM and FE model using an incremental approach.

data corresponding to the foldover stage will be briefly discussed next. Due to the occurrence of foldover, as shown in Fig 3, and due to a need to re-mesh during the iterative solutions of the FE model, the node in contact with the die at the top-plane changes during the entire course of deformation. We have used tracking points concept as shown in Fig. 3, to extract $H-D-d$ data from the FE solution. However, depending on the solution step, either of the tracking points P_1 to P_9 sequentially represent the contact point between the upper die and the sample and eventually one of these points at a time represents $H-d$ data.

Smoothing of the pseudo-H-d data. Due to the incremental nature of the FE solution, as shown in Fig. 4a, the $H-d$ data is not smooth. However, evaluation of B relies on the slope of $H-d$ data and therefore the stepped curve has to be smoothed before a reliable B can be calculated for the deformation step. As shown in Fig. 4a, a bi-quadratic polynomial (fourth-order) is used here to smoothen the data before estimating B. It is clear in Fig. 4a that "the foldover induced stepped behaviour" increases in the data when friction factor m increases from $m=0.1$ to $m=0.8$. To achieve reliable data for a high friction factor cases, it is suggested to use finer mesh. This increases the number of steps but reduces the run and rise in each step.

Fig. 4b shows the onset of foldover on the $H-d$ data results from the FE model. It can be seen that by increasing the fixed factor of friction, m, the foldover starts sooner during the test.

Based on the extracted $H-d-D$ data, barreling parameter B at top and mid-plane for different values of m was calculated and the results are shown in Fig. 5.

In Fig. 5, estimations of B at the top and mid-plane of the sample are shown for comparison. In the calculation of the friction factor, the estimated B at the top-plane is adopted as justified earlier in this work.

Results and verifications

Comparison of the calculated m with the pseudo-experimental friction factor

Since the tribological conditions can easily change during BCT, it is extremely difficult to directly measure m during the test. This explains why a virtual lab and pseudo experiments are used here which provides a reliable platform to verify the accuracy of the identified m based on Eq. 22.

This section presents and compares the pseudo-experimental results for a series of constant m compression tests with those calculated based on Extended Avitzur model and EPM. The calculations are performed in two ways: with large and small increments.

*Calculation of **m** with large increments*

In the first verification set, the predicted deformed geometries using FE simulations, listed in Table 1, were chosen as input for EA and EPM case studies. For each simulation scenario, the corresponding friction factor m_{EA} and m_{EPM} were calculated using EA and EPM methods respectively. Given the current deformed configuration of the sample from the FE solution [23], the key deformation parameters are used to calculate B and m for the current stage of deformation with respect to the sample's initial undeformed configuration. The data listed in Table 1 are used regarding the initial geometry D_0 and H_0 using the large increment definition of B.

One may argue that a large increment approach violates the path dependence condition of the deformation. This does not apply to our verification set 1, simply because the increment is not used to find the current deformed configuration but only to find the barreling parameter. The current deformed configuration is dictated by our finite element based virtual experiment which is independent of the step size chosen to calculate B.

*Calculation of **m** with small increments*

The pseudo-experimental $H-d$ data used in this section were generated using the second set of finite element simulations to (1)- demonstrate how barreling and m develop during a typical BCT test and (2)- test the accuracy of Eq. 22 in estimating m with an incremental approach to the deformation.

The results in Fig. 7 exclude the reductions with $H \leq 11$ due to the development of the foldover in this zone, as shown in Fig. 4b.

Results from a large number of finite element simulations, similar to those in Fig. 7, showed that the calculated friction factor m is very sensitive to B. According to [27], the $H-B$ curve becomes indeterminate near $H \to H_0$. A similar singularity also exists for the EA model [35]. This limitation has to be kept in mind when estimating B at the top-plane and at the early stages of the test. For the case presented in Fig. 5, the singularity exists near $H=16$ *mm*. EPM's barrelling parameter B, evaluated at the mid plane: $z=0$ and $2\bar{R} = D_n$, is singular when H and

H_0 are too close ($H_{n-1} \rightarrow H_n$) [26]. This leads to unrealistic values of friction factor. Excluding the foldover zone, $H \leq 12$ in Fig. 4b, and excluding a zone in the vicinity of the singularity, one should expect the most accurate estimations of m using Eq. 22 where $13 \leq H \leq 15$. The results in Fig. 7 confirm this postulate. Interestingly, the results in Fig. 6 indicate the presence of a minimum B within this accuracy zone i.e. with low to moderate reduction in H where $13 \leq H \leq 15$ mm. It is clear in Fig. 7 that the calculated m from Eq. 22 in the vicinity of the minimum are reasonably close to their nominated and fixed values in the FE simulations. A similar conclusion can be made for the results with large increments shown in Fig. 6a. It is evident from Fig. 7 that when the friction increases, the amplitude of the fluctuations in the estimated m around the nominal fixed value of the friction factor also increases.

Discussion and conclusions

The only available analytical solution for the test's friction factor, EA solution, relies on the sample's shape changes. While due to its convenience, the solution has been widely used for the last two decades, recent studies have revealed that it suffers serious limitation in terms of accuracy and applicability. A close examination of the EA method reveals that exact expression of the sample's profile in the method is not possible. Solhjoo proposed an examination method for EA's barreling parameter using a series expansion of the profile equation and suggested the limitation of Avitzur's family of the formulation is due to its chosen kinematically admissible velocity field which poorly represents the deformation. Also, the velocity field is incapable to capture the unavoidable foldover phenomenon. The presented results in this work (Fig. 6b). confirm that the limitation is inherent to the utilized velocity field in EA. Poor and inaccurate estimations of EA's friction factor, shown in Fig. 6b complies with previous findings by [23]; EA's family of barreled solutions are unqualified to model BCT's friction and to identify its friction factor. This emphasises the importance of the current work and similar family of formulations to enable more reliable estimation of the friction factor m.

The friction estimation shown in Figs. 6a and 8 comply reasonably well comply with the FE results.

A fixed finite element model was used for all simulations. The model is not optimized for all test scenarios. Mesh sizes and their aspect ratio have to be chosen following the compaction ratio. As a result, the accuracy of the FE solutions can change for the cases presented in Table 1. This can explain mixed compliance of the EPM and FE results.

BCT's finite element model served here as a reference to assess and compare the validity of EA and EPM. However, the finite element model cannot be used as a substitute for EA and EP models. This can be understood by noting that both EA and EPM are classified as characterization tools; given measured BCT's load displacement and deformed geometry data (as inputs), the characterization tool estimates friction factor and the flow data (as output). A finite element model, however, requires friction factor and flow data as input to estimate BCT's load-displacement response.

A key feature of the EPM based upper bound solution is the plastic power integral. The term found to be solvable analytically without rendering singularities in its domain or a need for numerical integration. Also, contrary to the EA solution, the EPM's barreling parameter can be calculated without a need to employ approximate solutions based on series expansion so on. Choosing the EPM velocity field and employing R has enabled the completion of the integration in a closed-form. Occasionally, analytical integration is impossible or singularities arise at $r = 0$ based on other velocity fields.

We presented here an alternative energy-based and closed-form solution to estimate the test's friction factor. A two-dimensional velocity field and its kinematic model were employed in the proposed friction solution which only requires BCT sample's initial and final dimensions as its inputs.

Contrary to the currently used BCT solutions, the proposed EPM solution requires only one experimental data set, "load-displacement-barreling data", to post-process and estimate both friction factor and flow behaviour.

It was demonstrated that other available solutions for the axisymmetric compression problem, known as CPMs, cannot identify the friction factor as both models require the friction factor as their input and have several known limitations. In contrast to the EA solution, EPM solution demonstrated a good agreement with finite element simulation of BCT for both incremental and generic formulations. Comparing the identified friction factors for several cases using EA and the proposed EPM, the latter solution was verified. It was also demonstrated that the factor identified using the EA model is inaccurate and therefore unreliable. The merits and disadvantages of the existing models and their solutions were discussed and compared with those presented in the current work. The presented EPM solution enabled to estimate the friction factor reliably outside the singularity and foldover zones. This justifies more applications of the current model for example in constitutive modelling and post-processing of the test data. A key feature of the presented solution is that "EPM's deformation power integral" can be solved analytically without a need for numerical integration. The proposed solution has been now verified at both the kinematic and constitutive levels. Due to the limitations of numerical solutions such as the finite element method for direct post-processing of mechanical test data, the presented closed-form solution is considered a significant analytical tool. The presented solution is a significant development in mechanical modelling and analysing the BCT data. Such developments should enable a more meaningful interpretation of the test data and a better understanding of the underlying deformation phenomena that are typically simulated by the compression test.

Declaration of Competing Interest

The author declares that there exists no conflict of interest or relationships that could potentially influence or bias this work.

Appendix A

Solving Eq. 21, friction factor m was identified and simplified as presented by Eq. 22. The solution and simplification involved lengthy and complex integrations and derivations in a symbolic fashion. To ensure the correctness of the solution, Wolfram Mathematica software was employed to numerically and symbolically verify the solution. The use of the software is beyond the scope of this paper and can be found elsewhere (e.g. [60,61]) and for the sake of brevity, only the simplification results are presented. However, the source files for Computer-Aided Algebra Software Mathematica which were used here are available upon request.

Equation 22 provides EPM's closed-form solution for m. The expression is too long to be used with an ordinary calculator. The relationship for friction factor as described by Eq. 22 can be easily integrated into an excel spreadsheet or in a code for data conversion, friction calculations and simulation. It is suggested to utilize the equation as a subroutine in a computational framework. Fig. A1 presents a Fortran subroutine (*findm.for*) for an easier utilization of EPM's closed-form solution of m (see Eq. 22). The subroutine requires instantaneous values of B, H and $\bar{R}$ as its inputs and returns the calculated value of m as the output. This allows to post-process the test data (e.g. to convert BCT's raw data into flow curve) by a geometry-based estimation of the friction factor m.

Credit authorship contribution statement

S. Khoddam: Conceptualization, Data curation, Formal analysis, Investigation, Methodology, Project administration, Resources, Software, Supervision, Validation, Visualization, Writing - original draft. **M. Fardi:** Conceptualization, Resources. **S. Solhjoo:** Conceptualization, Data curation, Formal analysis, Resources, Writing - review & editing.

```
c ************************************************************
          Subroutine findm(B,h,R,m)
          IMPLICIT  DOUBLE PRECISION (A-H, O-Z), INTEGER*4 (I-N)
c
c   B: barrelling parameter, h: current height, R: effective radius
c   Given B, h and R, this routine returns  friction coefficient; m
c
          m=(h*(-6*h**2*(Sqrt(3)*Sqrt(h**2*(-1 + B*h)**2) -
     &      Sqrt(3*h**2*(-1 + B*h)**2 + (1 - 2*B*h)**2*R**2)) -
     &    R**2*(4*Sqrt(3*B**2*h**4 + (1 - 2*B*h)**2*R**2) +
     &      Sqrt(3*h**2*(-1 + B*h)**2 + (1 - 2*B*h)**2*R**2)) -
     &      2*B**3*h**3*(3*h**2*(Sqrt(3)*Sqrt(B**2*h**4) +
     &      Sqrt(3)*Sqrt(h**2*(-1 + B*h)**2) - Sqrt(3*B**2*h**4 +
     &      (1 - 2*B*h)**2*R**2) - Sqrt(3*h**2*(-1 + B*h)**2 +
     &      (1 - 2*B*h)**2*R**2)) - 10*R**2*(Sqrt(3*B**2*h**4 +
     &      (1 - 2*B*h)**2*R**2) + Sqrt(3*h**2*(-1 + B*h)**2 +
     &      (1 - 2*B*h)**2*R**2)))+
     &      6*B**2*h**2*(h**2*(2*Sqrt(3)*Sqrt(B**2*h**4) +
     &      Sqrt(3)*Sqrt(h**2*(-1 + B*h)**2) - 2*Sqrt(3*B**2*h**4 +
     &      (1 - 2*B*h)**2*R**2) - Sqrt(3*h**2*(-1 + B*h)**2 +
     &      (1 - 2*B*h)**2*R**2)) - 2*R**2*(3*Sqrt(3*B**2*h**4 +
     &      (1 - 2*B*h)**2*R**2) + 2*Sqrt(3*h**2*(-1 + B*h)**2 +
     &      (1 - 2*B*h)**2*R**2))) +
     &       3*B*h*(2*h**2*(Sqrt(3)*Sqrt(h**2*(-1 + B*h)**2) -
     &      Sqrt(3*h**2*(-1 + B*h)**2 + (1 - 2*B*h)**2*R**2)) +
     &      R**2*(7*Sqrt(3*B**2*h**4 + (1 - 2*B*h)**2*R**2) +
     &      3*Sqrt(3*h**2*(-1 + B*h)**2 + (1 - 2*B*h)**2*R**2)))) -
     &      Sqrt(3)*(1 - 2*B*h)**4*R**4*(Log(-3*B*h**2 +
     &      Sqrt(9*B**2*h**4 + 3*(1 - 2*B*h)**2*R**2)) -
     &      Log(3*h*(-1 + B*h) + Sqrt(9*h**2*(-1 + B*h)**2 +
     &      3*(1 - 2*B*h)**2*R**2))))/(4.*h*(1 - 2*B*h)**4*R**3)
          Return
          End
```

Fig. A1. Fortran subroutine "*Findm.for*" to calculate friction factor *m*.

References

[1] Qi Y, Calahan KN, Rentschler ME, Long R. Friction between a plane strain circular indenter and a thick poroelastic substrate. Mech. Mater 2020;142:103303.
[2] Ben N-y, Zhang Q, Bandyopadhyay K, Lee M-G. Analysis of friction behaviour under oscillating forming process using T-shape compression test and finite element simulation. J. Mater. Process. Technol. 2020;275:116327.
[3] Lu J, Song Y, Hua L, Zhou P, Xie G. Effect of temperature on friction and galling behavior of 7075 aluminum alloy sheet based on ball-on-plate sliding test. Tribology International 2019;140:105872.
[4] Xu B, Qu J, Jin Q. Deformation behaviour of the hot upsetting cylindrical specimen with dynamic recrystallization. Int. J. Mech. Sci. 2006;48:190–7.
[5] Hu C, Yin Q, Zhao Z, Ou H. A new measuring method for friction factor by using ring with inner boss compression test. Int. J. Mech. Sci. 2017;123:133–40.
[6] Zhang L, Min J, Carsley JE, Stoughton TB, Lin J. Experimental and theoretical investigation on the role of friction in Nakazima testing. Int. J. Mech. Sci. 2017;133:217–26.
[7] Fereshteh-Saniee F, Pillinger I, Hartley P. Friction modelling for the physical simulation of the bulk metal forming processes, J. Mater. Process. Technol. 2004;153-154:151–6.
[8] Balasubramani S, Prem Kumar N, factor Friction. Load and Displacement Studies of AA6063 in forward Extrusion process with Equal Channel Angular Pressing (ECAP) Preprocess. Materials Today: Proceedings 2019;16:1333–7.
[9] Farhoumand A, Hodgson PD, Khoddam S, Fang XY. Multiple Pass Axi-symmetrical Forward Spiral Extrusion of Interstitial-Free (IF) Steel. Mater. Sci. Eng., A 2013;579:217–25.
[10] Velay V, Matsumoto H, Vidal V, Chiba A. Behavior modeling and microstructural evolutions of Ti-6Al-4V alloy under hot forming conditions. Int. J. Mech. Sci. 2016;108-109:1–13.
[11] Latypov MI, Lee M-G, Beygelzimer Y, Prilepo D, Gusar Y, Kim HS. Modeling and Characterization of Texture Evolution in Twist Extrusion. Metall. Mater. Trans. A 2016;47:1248–60.
[12] Fan XG, Dong YD, Yang H, Gao PF, Zhan M. Friction assessment in uniaxial compression test: A new evaluation method based on local bulge profile. J. Mater. Process. Technol. 2017;243:282–90.
[13] Hoyos E, López D, Alvarez H. A phenomenologically based material flow model for friction stir welding. Mater. Des. 2016;111:321–30.
[14] Christiansen P, Martins PAF, Bay N. Friction Compensation in the Upsetting of Cylindrical Test Specimens. Experimental Mechanics 2016;56:1271–9.
[15] Khodabakhshi F, Simchi A, Kokabi AH, Gerlich AP. Similar and dissimilar friction-stir welding of an PM aluminum-matrix hybrid nanocomposite and commercial pure aluminum: Microstructure and mechanical properties. Mater. Sci. Eng. A 2016;666:225–37.
[16] de Lima RP, Keller T. Impact of sample dimensions, soil-cylinder wall friction and elastic properties of soil on stress field and bulk density in uniaxial compression tests. Soil and Tillage Research 2019;189:15–24.
[17] Kobayashi S, Thomsen EG. Upper- and lower-bound solutions to axisymmetric compression and extrusion problems. Int. J. Mech. Sci. 1965;7:127–43.
[18] Avitzur B. Metal forming; processes and analysis. 1 ed. New York: McGraw-Hill; 1968.
[19] Avitzur B, Forming Metal. The Application of Limit Analysis. Annu. Rev. Mater. Sci. 1977;7:261–300.
[20] Avitzur B. Metal forming: the application of limit analysis. Marcel Dekker Inc; 1980.
[21] Avitzur B. A Keynote Presentation: A Personal Look on My Involvement in the Recent History of Metal Forming Research. Advanced Technology of Plasticity 1990;4:1–12.
[22] Ebrahimi R, Najafizadeh A. A new method for evaluation of friction in bulk metal forming. J. Mater. Process. Technol. 2004;152:136–43.
[23] Solhjoo S. A note on "Barrel Compression Test": A method for evaluation of friction. Comput. Mater. Sci. 2010;49:435–8.
[24] Fardi M, Ibrahim R, Hodgson PD, Khoddam S. A new horizon for Barrelling Compression Test; Exponential Profile Modelling. J. Adv. Mater., adem 2017;201700328:11.
[25] Khoddam S, Hodgson PD. Advancing Mechanics of Barrelling Compression Test. Mech. Mater. 2017;122:8.
[26] Khoddam S. Deformation under combined compression and shear: a new kinematic solution. J. Mater. Sci. 2018;54:4754–65.
[27] Khoddam S, Solhjoo S, Hodgson PD. A power-based approach to assess the barrelling test's weak solution. Int. J. Mech. Sci. 2019;161-162:105033.

[28] Nadai A. Plastic behavior of metals in the strain-hardening range. Part I, J. Appl. Phys. 1937;8:205–13.
[29] Sofuoglu H, Rasty J. On the measurement of friction coefficient utilizing the ring compression test. Tribology International 1999;32:327–35.
[30] Sofuoglu H, Gedikli H. Determination of friction coefficient encountered in large deformation processes. Tribology International 2002;35:27–34.
[31] Stein E. History of the finite element method–mathematics meets mechanics–part I: Engineering developments. The History of Theoretical, Material and Computational Mechanics-Mathematics Meets Mechanics and Engineering. Springer; 2014. p. 399–442.
[32] Singh G, Bhandakkar TK. Semianalytical study of the effect of realistic boundary conditions on diffusion induced stresses in cylindrical lithium ion electrode-binder system. Int. J. Mech. Sci. 2019;163:105141.
[33] Gu Y, Zhang C, Qu W, Ding J. Investigation on near-boundary solutions for three-dimensional elasticity problems by an advanced BEM. Int. J. Mech. Sci. 2018;142-143:269–75.
[34] Fil'shtinskii L, Synah M, Kirichok T. Time-harmonic boundary value problem of coupled thermoelasticity and related integral equations method. Int. J. Mech. Sci. 2016;115-116:157–67.
[35] Solhjoo S, Khoddam S. Evaluation of barreling and friction in uniaxial compression test: A kinematic analysis. Int. J. Mech. Sci. 2019;156:486–93.
[36] Jung KH, Lee HC, Kim DK, Kang SH, Im YT. Friction measurement by the tip test for cold forging. Wear 2012;286-287:19–26.
[37] Abushawashi Y, Xiao X, Astakhov V. A novel approach for determining material constitutive parameters for a wide range of triaxiality under plane strain loading conditions. Int. J. Mech. Sci. 2013;74:133–42.
[38] Khoddam S, Hodgson PD. The need to revise the current methods to measure and assess static recrystallization behavior. Mech. Mater. 2015;89:85–97.
[39] Zhao K, Wang L, Chang Y, Yan J. Identification of post-necking stress–strain curve for sheet metals by inverse method. Mech. Mater. 2016;92:107–18.
[40] Sanchez-Camargo C-M, Hor A, Mabru C. A robust inverse analysis method for elasto-plastic behavior identification using the true geometry modeling of Berkovich indenter. Int. J. Mech. Sci. 2020;171:105370.
[41] Pereira FAM, de Moura MFSF, Dourado N, Morais JJL, Xavier J, Dias MIR. Determination of mode II cohesive law of bovine cortical bone using direct and inverse methods. Int. J. Mech. Sci. 2018;138-139:448–56.
[42] De Bono DM, London T, Baker M, Whiting MJ. A robust inverse analysis method to estimate the local tensile properties of heterogeneous materials from nano-indentation data. Int. J. Mech. Sci. 2017;123:162–76.
[43] Vieira DAG, Lisboa AC. Line search methods with guaranteed asymptotical convergence to an improving local optimum of multimodal functions. European Journal of Operational Research 2014;235:38–46.
[44] Lim S, Zhu J. Integrated data envelopment analysis: Global vs. local optimum. European Journal of Operational Research 2013;229:276–8.
[45] Kuo Y-C, Lee T-L. Tracking local optimality for cost parameterized optimization problems. Comput. Phys. Commun. 2014;185:572–7.
[46] Wang X, Li H, Chandrashekhara K, Rummel S, Lekakh S, Van Aken D, O'Malley R. Inverse finite element modeling of the barreling effect on experimental stress-strain curve for high temperature steel compression test. J. Mater. Process. Technol. 2017;243:465–73.
[47] Li Y, Onodera E, Chiba A. Evaluation of friction coefficient by simulation in bulk metal forming process. Metall. Mater. Trans. A 2010;41:224–32.
[48] Annasamy M, Haghdadi N, Taylor A, Hodgson P, Fabijanic D. Static recrystallization and grain growth behaviour of Al0.3CoCrFeNi high entropy alloy. Mat. Sci. Eng., A 2019;754:282–94.
[49] Jenab A, Karimi Taheri A. Experimental investigation of the hot deformation behavior of AA7075: Development and comparison of flow localization parameter and dynamic material model processing maps. Int. J. Mech. Sci. 2014;78:97–105.
[50] Shang X, Cui Z, Fu MW. A ductile fracture model considering stress state and Zener–Hollomon parameter for hot deformation of metallic materials. Int. J. Mech. Sci. 2018;144:800–12.
[51] Wolfson R. Essential University Physics: Pearson New International Edition. Pearson Higher Ed; 2013.
[52] Bonet J, Wood RD. Nonlinear continuum mechanics for finite element analysis. 2nd ed. Cambridge university press; 2008.
[53] Kobayashi S, Oh S-I, Altan T. Metal forming and the finite element method. New York: Oxford University press; 1989.
[54] Kupradze V, Aleksidze MA. The method of functional equations for the approximate solution of certain boundary value problems. USSR Computational Mathematics and Mathematical Physics 1964;4:82–126.
[55] Wang S, Ramaekers J. Measurement of friction and material flow-stress by a plane-strain compression tribometer. J. Mater. Process. Technol. 1996;57:345–50.
[56] Han H. Determination of Flow Stress and Coefficient of Friction for Extruded Anisotropic Materials under Cold Forming Conditions. Industriell produktion 2002.
[57] Reiss W, Pöhlandt K. THE RASTEGAEV UPSET TEST-A METHOD TO COMPRESS LARGE MATERIAL VOLUMES HOMOGENEOUSLY. Experimental Techniques 1986;10:20–4.
[58] Pöhlandt K. Materials testing for the metal forming industry. Berlin Heidelberg: Springer-Verlag; 1989.
[59] Rasmussen S, Nester W, Pöhlandt K. A further development of the Rastegaev upsetting test for measuring flow curves. Zeilschrift fuer Industrielk Fertigung 1984;74:667–70.
[60] Lutovac M, Tošić D. Symbolic analysis and design of control systems using Mathematica. International Journal of Control 2006;79:1368–81.
[61] Zitko R. SNEG-Mathematica package for symbolic calculations with second-quantization-operator expressions. arXiv preprint arXiv; 2011. p. 1105.4697.